

Theoretical study of doped-Tl₂Mn₂O₇ and Tl₂Mn₂O₇ under pressure

Molly De Raychaudhury¹, T. Saha-Dasgupta¹ and D. D. Sarma^{2,3,*}

¹ *S.N. Bose National Centre for Basic Sciences, Kolkata 700098, India*

² *Indian Association for the Cultivation of Science, Jadavpur, Kolkata 700032, India and*

³ *Solid State and Structural Chemistry Unit, Indian Institute of Science, Bangalore-560012, India*

(Dated: February 6, 2008)

Using first-principles density functional based calculations, we study the effect of doping and pressure in manganese based pyrochlore compound, Tl₂Mn₂O₇ that exhibits colossal magneto-resistive behavior. The theoretical study is motivated by the counter-intuitive experimental observation of suppression of ferromagnetic transition temperature upon application of pressure and its enhancement upon substitution of Mn by moderate amount of nonmagnetic Sb ion. We also attempt to resolve the issue related to crystal structure changes that may occur upon application of pressure.

I. INTRODUCTION

Manganese-based pyrochlore compounds such as Tl₂Mn₂O₇, form an interesting class of compounds which despite having similar colossal magneto-resistive (CMR) effect exhibit markedly different features compared to that of manganites. In contrast to manganites, these compounds are not mixed-valent, do not have any appreciable Jahn-Teller distortion¹ and seemingly show metallic behavior² both below and above the magnetic transition temperature T_c (≈ 140 K). Concerning the metallic behavior above T_c though, it is not totally clear whether it is a good metal or more like a bad metal or an insulator-like compound which arises due to difficulties related to sample preparation and defects present in the paramagnetic phase. Though the original data by Shimakawa et. al.² suggests the metallic behavior above T_c , the optical conductivity data³ and photoemission and x-ray absorption⁴ near edge spectroscopy point towards an insulator-like behavior in the paramagnetic regime. These non-manganite like features rule out the generally applicable double exchange mechanism or polaronic mechanism as the driving mechanism of ferromagnetism in this class of compound, and remained a mystery for quite some time. In absence of double exchange mechanism, a strong contestant for the driving mechanism is the Mn-O-Mn mediated superexchange mechanism, particularly since Mn-O-Mn form an angle⁵ of 133° , significantly smaller than 180° . This is however contradicted by the experimental findings that the ferromagnetic T_c gets suppressed by application of pressure⁶ and gets enhanced by moderate amount of introduction of nonmagnetic ion like Sb in place of Mn⁷. Employing N-th order muffin tin orbital (MTO) based NMTO-downfolding technique⁸, we have recently established⁹ that driving mechanism of ferromagnetism in this class of compounds is neither super-exchange or double-exchange, nor any exotic mechanism with nearest neighbor (NN) antiferromagnetic (AFM) coupling dominated by long-ranged ferromagnetic (FM) interaction¹⁰, but a kinetic energy assisted mechanism similar to that of double perovskite compounds like Sr₂FeMoO₆, Sr₂FeReO₆^{11,12} and Mn-doped GaAs¹³.

In the present paper, we give a detail account of the doping effect and the pressure effect from the electronic structure point of view, which lend further support to the existence of the proposed kinetic energy driven mechanism in these compounds. While the changes that happen in the crystal structure upon doping is clear, the situation is rather ambiguous in case of application of pressure. The initial measurement hinted to a decrease in Mn-O-Mn bond angle^{6,14} alongwith the compression of Mn-O bondlength. However the subsequent measurement¹⁵ indicated an increase in Mn-O-Mn bond angle which was used in terms of super exchange mechanism to explain the decrease in T_c . In view of these conflicting claims, we also take the opportunity to theoretically address the effect of pressure on the structure of Tl₂Mn₂O₇ and its implication on magnetism by detailed electronic structure calculations together with structural relaxations under pressure.

The rest of the paper is organized in the following way. Section II deals with various methodologies that have been employed to compute the crystallographic structure (in case of Tl₂Mn₂O₇ under pressure) and to compute and analyze the subsequent electronic structure of Tl₂Mn₂O₇ under doping and pressure. In section III, we present our results. This section is divided into several subsections. In section IIIA, the electronic structure of pristine Tl₂Mn₂O₇ is presented and the proposed kinetic energy driven mechanism is introduced as a reference, which will form the basis of discussion in the following. Section IIIB is devoted to Tl₂Mn₂O₇ under pressure, while section IIIC is devoted to Sb-doped Tl₂Mn₂O₇. Finally, we conclude the paper with a summary presented in section IV.

II. METHODOLOGY

We have investigated the electronic structure of pure Tl₂Mn₂O₇, Tl₂Mn_{2-x}Sb_xO₇ and Tl₂Mn₂O₇ under pressure by the tight-binding linear muffin-tin orbital (LMTO)¹⁶ method, computed within the framework of the local spin density approximation (LSDA) of the density functional theory (DFT). The employed basis set, consisted of Tl-6s, 6p and 5d states, Mn-4s, 4p and 3d

states, and O-2s and 2p states. Three different classes of empty spheres were used to fill up the space. The self-consistent calculations were performed on a BZ mesh of $12 \times 12 \times 12$.

The computed band structures were analyzed and interpreted in terms of NMTO-downfolding technique⁸. The NMTO technique, introduced and implemented in recent years, goes beyond the scope of standard LMTO technique by defining an energetically accurate basis with consistent description throughout the space involving both the MT spheres and the interstitial. As important feature of this technique is the energy-selective downfolding procedure where one integrates out degrees of freedom and keeps only few degrees of freedom active to define a few-orbital, low-energy Hamiltonian. The effective NMTOs defining such Hamiltonian, serve as the Wannier or Wannier-like function corresponding to the selected low-energy bands.

For the calculation of the exchange interaction strengths, J , a supercell involving a sixteen Mn atoms was constructed which amounts to enlarging the original unit cell by four times. This was achieved by replacing the original face centered cubic (FCC) lattice by the simple cubic lattice with four times as many atoms as that in FCC. The basic structural unit of Mn sublattice is the Mn_4 tetrahedra which share corners to form an infinite 3D lattice. We calculated the LSDA total energies by considering different magnetic configurations of this sublattice. In total, six spin configurations have been chosen. One of the six configurations was FM and the other five were AFM. The details of the spin configurations chosen are as given in Table I in ref⁹. The total energies are then mapped on to an effective Heisenberg Hamiltonian formed by the Mn^{+4} spins. The Hamiltonian considered till the 3NN(third nearest neighbor) interactions is:

$$H = J_1 \sum_{nn} S_i \cdot S_j + J_2 \sum_{2nn} S_i \cdot S_j + J_3 \sum_{3nn} S_i \cdot S_j \quad (1)$$

where S_i denoted the spin-3/2 operator corresponding to the Mn^{+4} spins at the site i , and J_1, J_2 and J_3 denote the NN, 2NN(second nearest neighbor) and 3NN magnetic exchange interaction strengths. Since we have restricted ourselves to only five AFM configurations amongst many possible AFM configurations, we computed seven different estimates of these J 's along with their standard deviations employing set of three energy differences chosen out of total five different energy differences. This limitation can be overcome by taking as many AFM spin configurations as practically possible. The mean-field estimate of T_c is given by

$$T_c^{mf} = \frac{S(S+1)}{3k_B} J_0 \quad (2)$$

where J_0 , is the net effective magnetic exchange interaction, given by

$$J_0 = z_1 J_1 + z_2 J_2 + z_3 J_3 \quad (3)$$

and $S = \frac{3}{2}$. k_B is the Boltzman constant and z_1, z_2, z_3 are the number of NN, 2NN and 3NN Mn pairs. For undoped $\text{Tl}_2\text{Mn}_2\text{O}_7$, $z_1 = 6$, $z_2 = 12$ and $z_3 = 12$. However, these numbers change in case of doped calculations where some of the Mn atoms gets replaced by the nonmagnetic Sb ion and therefore do not contribute in the calculation of magnetic energy. The application of mean-field theory is naturally expected to overestimate the T_c . Use of Monte Carlo simulation¹⁷ or Green Function method¹⁸ can give better estimates and agreements with experimentally measured values. One needs to keep this in mind when comparisons are being made with the measured T_c in the following sections.

$\text{Tl}_2\text{Mn}_2\text{O}_7$ occurs in cubic, face-centered lattice with $Fd-3m$ space group and two formula unit in the cell.⁵ There are two types of oxygen, O' and O. While O oxygens provide the octahedral surrounding of the Mn atom which corner share to give rise to a geometry of a closed ring or cage, O' atoms form nearest neighbor bonds with Tl giving rise to $\text{Tl}_2\text{O}'$ complex running through the cage like geometry as shown in left panel of Fig. 1. The structural parameters for the pristine $\text{Tl}_2\text{Mn}_2\text{O}_7$, and Sb-doped $\text{Tl}_2\text{Mn}_2\text{O}_7$ have been taken as the experimentally determined structure published in literature^{7,19}. However, as mentioned already, the structural information for $\text{Tl}_2\text{Mn}_2\text{O}_7$ under pressure is somewhat controversial which calls for structural optimization. For this purpose, we have adopted the pseudopotential method²⁰ as implemented in the VASP²¹ code. We have employed the pseudopotentials generated by the projector-augmented wave (PAW)²² method. Wavefunctions have been expanded in terms of plane waves with a cut off energy of 400 eV. A k -mesh of $6 \times 6 \times 6$ was employed to perform the self-consistent calculations. In $\text{Tl}_2\text{Mn}_2\text{O}_7$, Tl, Mn, O' and O atoms occupy the Wyckoff positions, 16d, 16c, 8b and 48f respectively. Among these only the positions given by 48f contain the internal parameter, u . This parameter u defines the $\angle \text{Mn-O-Mn}$ (see right panel of Fig.1). As u increases, the $\angle \text{Mn-O-Mn}$ decreases and vice versa. When pressure is applied, it needs to be investigated whether the u parameter also varies along with the reduction in the bondlengths. If at all it changes, it has to be ascertained in what way it does so. In our calculation, the O position is relaxed by varying u , in order to find out the variation of total energy with angle formed between Mn, O and Mn atoms. In order to obtain the theoretical ground state, cohesive properties and estimate the pressure, Murnaghan²³ equation of state has been employed to fit the LSDA total energies. The Murnaghan equation of state is given by

$$E(V) = E_0 + \frac{B_0 \cdot V}{B'_0} \left[\frac{(V_0/V)^{B'_0}}{B'_0 - 1} + 1 \right] - \frac{B_0 \cdot V_0}{B'_0 - 1} \quad (4)$$

where V_0 is the equilibrium volume, B_0 is the bulk modulus and is given by $B_0 = -V(\delta P/\delta V)_T$ evaluated at volume V_0 . B'_0 is the pressure derivative of B_0 also evaluated at volume V_0 . B'_0 provides a measure of stiffness

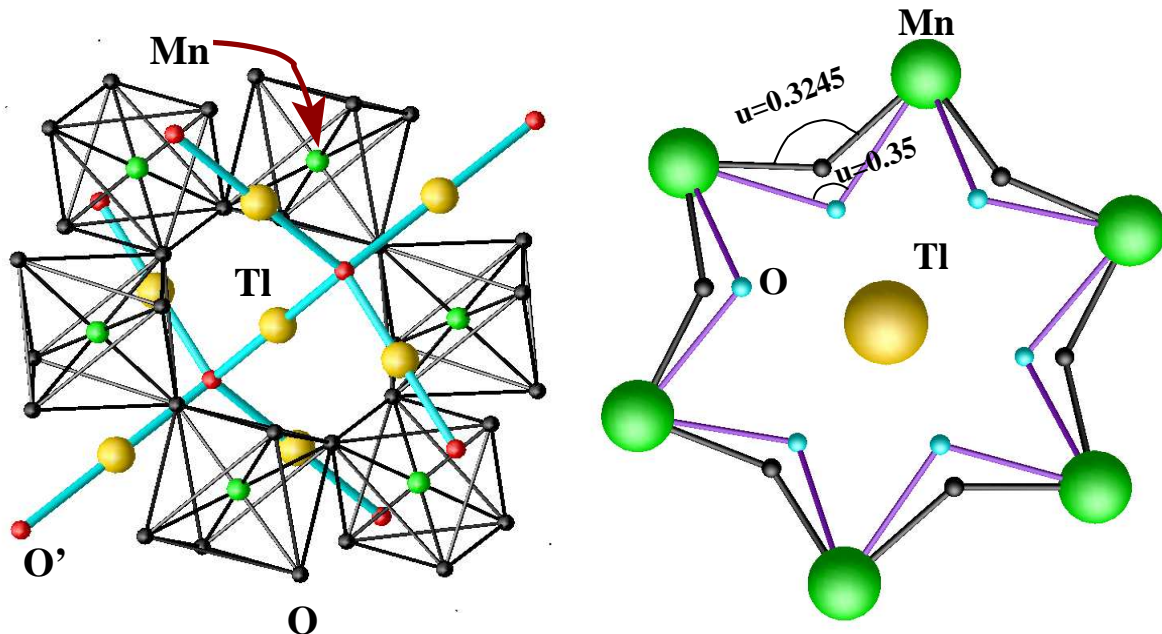


FIG. 1: (color on-line) Left panel: The $\text{Tl}_2\text{Mn}_2\text{O}_7$ structure consisting of the ring formed by MnO_6 octahedra with Tl-O' rods passing through the holes of the rings. Right panel: Backbone of the structure realized by the ring like structure formed by the Mn-O-Mn network (the Tl-O' rod network is not shown for clarity). Gold, green and black or cyan spheres denote the Tl, Mn and O atoms. Black and cyan spheres correspond to oxygen (O) atoms with two different oxygen (O) position parameter u .

of the material upon increasing pressure. Typical values for the parameter B'_0 are between 4 and 7. Pressure, P , corresponding to volume, V , occupied by a cell of a particular lattice parameter is given by

$$P(V) = \frac{B_0}{B'_0} \left[(V_0/V)^{B'_0} - 1 \right] \quad (5)$$

III. RESULTS

A. FM Electronic Structure of Pristine $\text{Tl}_2\text{Mn}_2\text{O}_7$ and the Underlying Mechanism

The LSDA electronic structure of ferromagnetically ordered $\text{Tl}_2\text{Mn}_2\text{O}_7$, computed with TB-LMTO method is shown in Fig.2. This figure shows both the band structure and the orbital projected density of states (DOS). Consistent with the nominal valence of O^{2-} and Mn^{4+} , oxygen dominated states are totally occupied, while the crystal field split $\text{Mn } t_{2g}$ states are occupied in the majority spin channel and close to empty in the minority spin channel. $\text{Mn } e_g$ states consistent with $3d^3$ configuration of Mn, remain empty in both the spin channels. Tl bands, consistent with Tl^{3+} nominal valence also remain almost empty. However, interestingly in the majority spin channel, the Tl-6s state mixed with O'-2p states overlap with $\text{Mn } e_g$ manifold spanning an energy range of about 2-4 eV²⁴, while in the minority spin channel, they overlap with nearly empty $\text{Mn } t_{2g}$ dominated states, which give rise to highly dispersive band in bottom of this manifold,

crossing the Fermi level, E_F , as seen in lower, left panel of Fig.2. This hints to a large spin-splitting at the Tl site. This is unusual in the sense, one would normally expect Tl to be essentially nonmagnetic with tiny spin splitting. This unusual feature plays the key role in providing the understanding of the driving mechanism of ferromagnetism in $\text{Tl}_2\text{Mn}_2\text{O}_7$. This has been explained in detail in ref⁹. As has been shown in ref⁹, the unhybridized effective Tl-O' level is positioned in between the spin-split $\text{Mn } t_{2g}$ states and on turning on the hybridization, it induces a renormalized spin-splitting within the Tl-O' level which is directed in a opposite way compared to the spin-splitting at the Mn site. This happens due to pushing up of the Tl-O' spin-up state and pushing down of the Tl-O' spin-down states, driven by coupling with the $\text{Mn } t_{2g}$ states of the same symmetry. The energy gain contributed by this hybridization induced negative spin polarization of the otherwise nonmagnetic element, is the central concept in this novel mechanism. This mechanism ensures a specific spin orientation between the localized $\text{Mn } t_{2g}$ spins and the mobile carrier formed by the hybridized renormalized state, which in turn aligns the spins in Mn sublattice. This is a general mechanism and found to be operative in case of a number of compounds like $\text{Sr}_2\text{FeMoO}_6$, $\text{Sr}_2\text{FeReO}_6$ ^{11,12}, Mn-doped GaAs¹³ and CuCr_2S_4 ²⁵ etc.

In the following subsections, we will present a detail account of the changes in the electronic structure and the variation in T_c of $\text{Tl}_2\text{Mn}_2\text{O}_7$ with doping and under pressure. We will argue that the counter-intuitive variation in T_c has its origin in the modified electronic structure

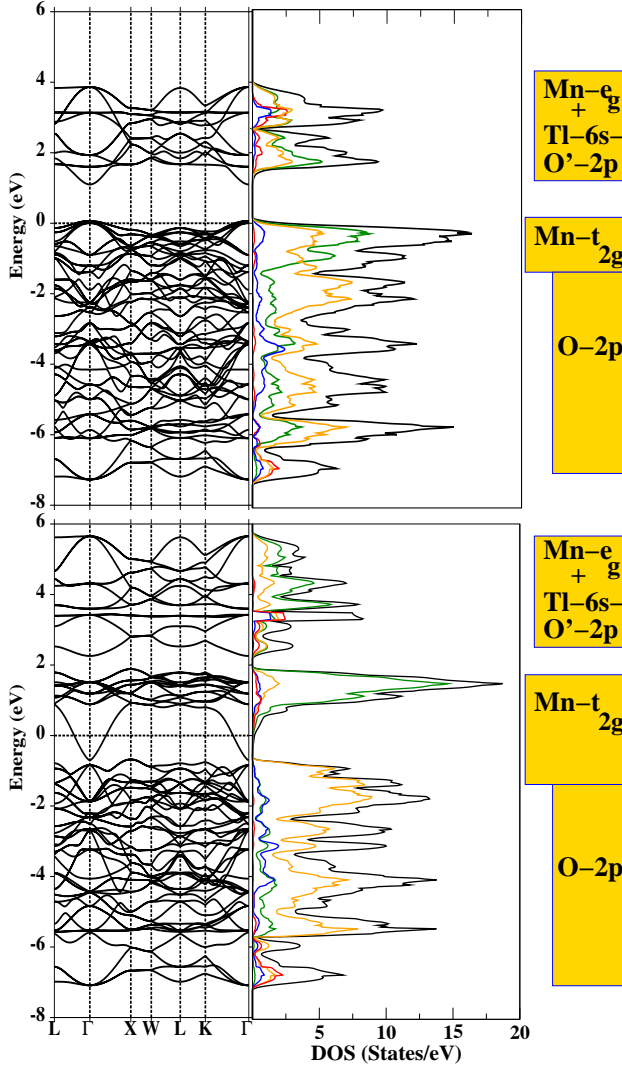


FIG. 2: (color on-line) Left panels show the spin-polarized band structure computed within LSDA for $\text{Tl}_2\text{Mn}_2\text{O}_7$. The zero of the energy is set at the LSDA Fermi energy, E_F . Right panels give the spin-polarized total (black), Tl-6s (red), Mn-3d (green), O-2p (orange) and O'-2p (blue) density of states. Upper and the lower figures correspond to the majority and minority spin contributions respectively in both the panels. Bars on the right signify the energy range for which various characters dominate.

and follows naturally from the framework of proposed hybridization induced mechanism of ferromagnetism as was established in ref⁹ and reviewed in the above.

B. $\text{Tl}_2\text{Mn}_2\text{O}_7$ under pressure

As explained before, to investigate $\text{Tl}_2\text{Mn}_2\text{O}_7$ under pressure one needs to first settle the issues related to crystal structure. To be precise, does applied pressure increase or decrease or not alter the $\angle\text{Mn-O-Mn}$? For this

purpose, we have carried out a series of structural optimization calculations with pseudopotential method²⁰. At first the cohesive properties were calculated within LSDA. Following the recent claim²⁷ that application of on-site U can also influence the cohesive properties of transition metal oxides, we have repeated our calculations also with LSDA+ U functional.

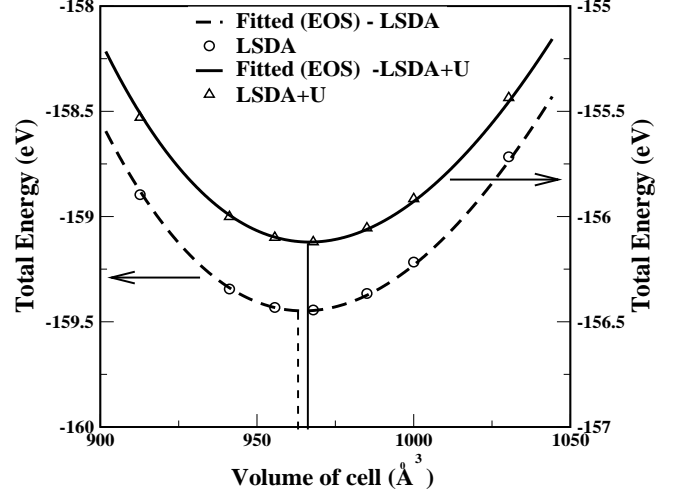


FIG. 3: Total energy vs. volume of the unitcell calculations within LSDA and LSDA+ U . The symbols denote the DFT total energies and the solid and dashed lines depict the total energies obtained from fitting with Murnaghan²³ equation of state (EOS).

LSDA total energy vs volume calculation, shown in Fig.3, has a minimum corresponding to lattice constant of 9.881 Å. Considering the experimental value of the lattice constant is 9.892 Å, this gives a deviation of about 0.1 %, which is within the limit of LSDA overbinding. The value of the bulk modulus, obtained by fitting the total energy vs volume curve with Murnagahan equation of state²³ is 230.6 GPa, which is of the same order as the experimentally measured value of ≈ 200 GPa in $\text{Tl}_{1.8}\text{Cd}_{0.2}\text{Mn}_2\text{O}_7$ ¹⁵. B_0 is +4.84, much higher than that in Cd doped $\text{Tl}_2\text{Mn}_2\text{O}_7$ but within the expected limit. Applying an on-site Coulomb interaction of $U=2$ eV and $J=0.7$ eV on the Mn site leads to a slightly better agreement with the experimental values. The lattice parameter changes to 9.888 Å, B_0 and B'_0 remain unaltered. In view of the slightly improved results of LSDA+ U , we have used the B_0 and B'_0 as estimated by LSDA+ U calculations to compute the pressure as given by Eq.(5).

Till now we have considered the experimental $\angle\text{Mn-O-Mn}$ as the one for the theoretical ground state. One needs to relax this angle in order to obtain the true theoretically predicted ground state. The co-ordinate of O atom in the basis is given by $(u, .125, .125)$. The u parameter will push O atom in or out depending on its value, thereby changing the angle formed between Mn, O and Mn atoms. The u parameter is relaxed in the subsequent calculations, and the LSDA (for 9.881 Å) and LSDA+ U total energies

	LDA	LSDA+U	EXPT.
$a(\text{\AA})$	9.881	9.888	9.892
u	0.3214	0.3227	0.3254
Mn-O (\AA)	1.886	1.890	1.901
$\angle \text{Mn}-\text{O}-\text{Mn}(\text{deg})$	136.01	135.29	133.8
B_0 (GPa)	230.6	230.7	
B'_0	+4.84	+4.85	

TABLE I: Calculated ground state structural parameters of $\text{Ti}_2\text{Mn}_2\text{O}_7$ within LSDA and LSDA+U compared with the experimental⁵ data at ambient condition.

(for 9.888 \AA) are computed varying the u parameter. The minimum in the E vs u curve (see Fig.4) is obtained for $u=0.3214$ and 0.3227 respectively. The $\angle \text{Mn}-\text{O}-\text{Mn}$ in the ground state obtained within LSDA and LSDA+U framework are given in Table I along with the corresponding experimental values. Slightly better results are obtained for the LSDA+U calculations, a trend already observed in calculation for equilibrium lattice constant. The result match with experimental values upto the second decimal point for u and within 1.5° for Mn-O-Mn angle.

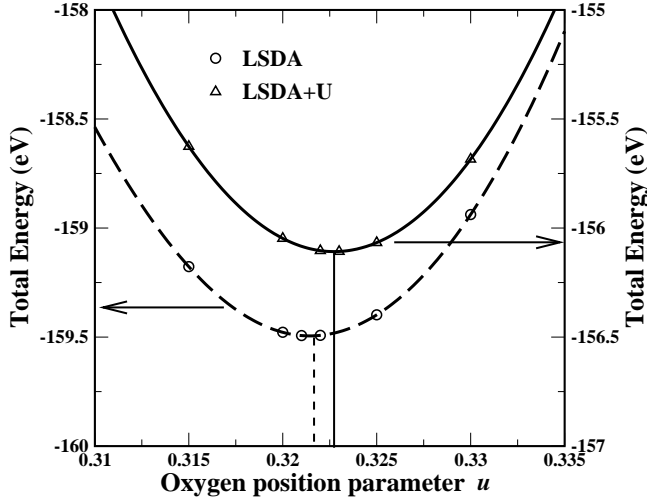


FIG. 4: Relaxation of the Oxygen-O position parameter u at ambient condition within LSDA and LSDA+U in $\text{Ti}_2\text{Mn}_2\text{O}_7$. The symbols are the DFT total energies and the solid and dashed lines are cubic spline interpolated.

Having established the ground state, in the next step we relax the O position for lattice parameters $a=9.846$ and 9.69 \AA (LSDA+U) which amount to applying a pressure of 3.04 GPa and 16.28 GPa. This will clarify whether the Mn-O-Mn angle also changes with the decrease in the interatomic distances. The minimum obtained from the total energy vs. u plots, as shown in Fig. 5 are listed in Table II. We find that on application of pressure, the $\angle \text{Mn}-\text{O}-\text{Mn}$ reduces *insignificantly*, by about 0.1° and 0.4° for pressure of 3.04 GPa and 16.28 GPa respectively. A reduction of the angle by about 0.6° occurs for the same applied pressure (16.28 GPa) within LSDA. We thereby

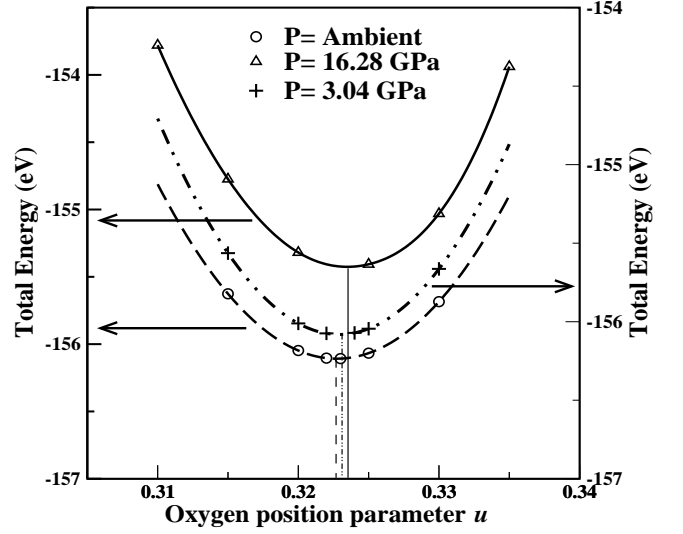


FIG. 5: Total energy vs u , i. e. relaxation of the Oxygen (O) position parameter u at ambient condition and under pressure of 3.04 and 16.28 GPa within LSDA+U in $\text{Ti}_2\text{Mn}_2\text{O}_7$. The symbols are the DFT total energies and the solid, dashed and dashed-dotted lines are cubic spline interpolated.

	AMBIENT	3.04 GPa	16.28 GPa
u	0.3227	0.3230	0.3234
Mn-O(\AA)	1.890	1.883	1.854
$\angle \text{Mn}-\text{O}-\text{Mn}(\text{deg})$	135.29	135.18	134.90

TABLE II: Structural parameters obtained within LSDA+U at ambient and two different pressures upon relaxation of the Oxygen(O) position parameter u in $\text{Ti}_2\text{Mn}_2\text{O}_7$.

establish that, regardless of kind of DFT one is using, on applying pressure $\angle \text{Mn}-\text{O}-\text{Mn}$ does not increase rather decreases though almost insignificantly. The major effects comes from reduction in the bondlengths. In the following calculations, we have therefore kept the $\angle \text{Mn}-\text{O}-\text{Mn}$ unchanged upon application of pressure.

We have carried out LSDA total energy calculations for various spin arrangements of Mn atoms as explained in section II. The relative LSDA total energies, as given in Table III are mapped on to Eq. (1) in order to extract the J 's. The magnetic exchange interaction strengths are calculated and shown in Table IV for almost 2 % reduction in experimental lattice parameter, amounting to a pressure of 16.28 GPa. Considering pressure of 16.28 GPa, we observe a substantial decrease in the NN FM interaction. The 2 and 3 NN interactions remain almost the same. This leads to a mean-field T_c of about 140 K, leading to a decrease of about 41 K. The gradient is about -2.5 K/GPa. The gradient calculated from another set of calculations at 3.04 GPa is about -2.3 K/GPa. One can approximate a linear relation between T_c and applied pressure. Thus the average gradient is about -2.4 K/GPa. This is not an unreasonable estimate considering the mean-field overestimation. The ratio of exact T_c

	$\Delta E(\text{meV})$		
	Normal	3.04 GPa	16.28 GPa
FM	0	0	0
AFM1	9.55	9.18	7.36
AFM2	13.98	14.17	13.05
AFM3	12.24	11.49	8.82
AFM4	17.59	22.5	16.24
AFM5	18.39	17.7	14.04

TABLE III: Relative LSDA energies per Mn ion in meV in FM and five AFM spin configurations for $\text{Ti}_2\text{Mn}_2\text{O}_7$ at normal, 3.04 GPa and 16.28 GPa pressures. All energies are converged upto 0.01 meV per Mn ion.

and T_c^{mf} is estimated as 0.79 and 0.81 for BCC and FCC lattice with coordination 8 and 12 respectively. Considering the average coordination of 10 for Mn sublattice in $\text{Ti}_2\text{Mn}_2\text{O}_7$, one would expect the gradient in T_c to be about -1.9 K/GPa. This is a bit larger than the experimental values, which are -1.6 K/GPa⁶ and about -1 K/GPa¹⁵. A plausible explanation for this somewhat overestimation may be due to computational limitations imposed by the number of spin configurations. A better estimate of the gradient might have been reached had all the possible spin configurations been considered for calculation of the J's. Therefore one can conclude that within the limitation of our method, we have established the trend in ferromagnetism of $\text{Ti}_2\text{Mn}_2\text{O}_7$ with applied pressure correctly.

Pressure Appl.	J_1	J_2	J_3	J_0	T_c^{mf}
(GPa)	(meV)	(meV)	(meV)	(meV)	(K)
0	-2.52	-0.11	+0.33	12.48	181
3.04	-2.48	-0.16	+0.40	12.06	174
16.28	-1.99	-0.16	+0.35	9.66	140

TABLE IV: NN, 2NN, 3NN and effective exchange interaction strengths and mean-field Curie Temperature calculated within LSDA at ambient condition and at 3.04 and 16.28 GPa for $\text{Ti}_2\text{Mn}_2\text{O}_7$.

In Fig.6 we show the density of states of $\text{Ti}_2\text{Mn}_2\text{O}_7$ under 16.28 GPa pressure alongwith that of $\text{Ti}_2\text{Mn}_2\text{O}_7$ under ambient pressure for comparison. Upon application of pressure, the bondlengths shorten which enhances the Mn-O and Ti-O' interaction and as a result net bandwidth expands and t_{2g} - e_g splitting enhances. However the key effect is seen in the inset, where we show the Mn-d and Ti-s projected density of states in an energy window close to E_F in solid and dashed lines respectively. They are shown in two different colors, corresponding to ambient and 16.28 GPa pressure. We notice that the relative proportion of Ti-O' in the hybridized, dispersive band has reduced significantly upon application of pressure. It has reduced from 45 % in case of ambient pressure to 36 % in case of 16.28 GPa pressure. This indicates reduction of Mn-Ti-O' hybridization upon application of

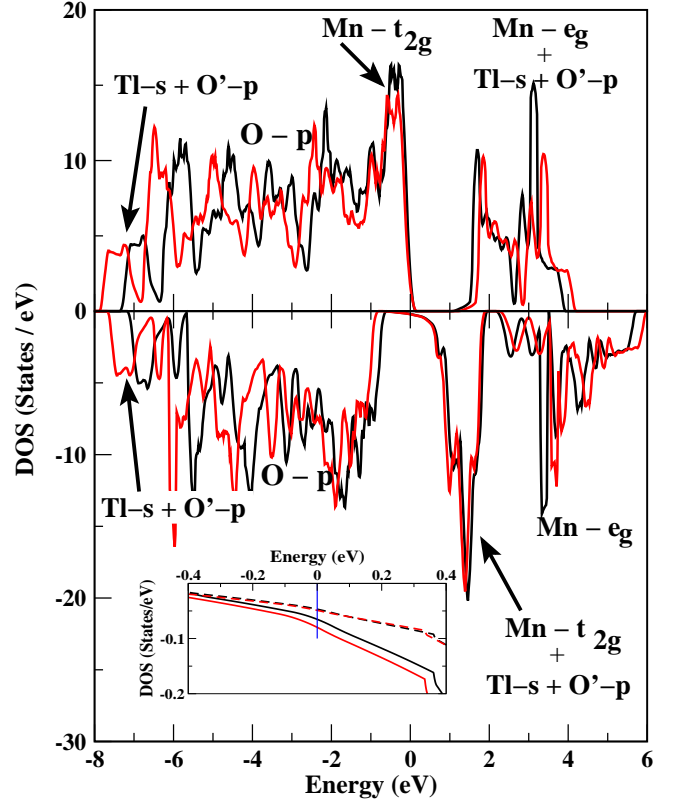


FIG. 6: (color on-line) Spin-polarized density of states at ambient condition (black) and 16.28 GPa (red) calculated within LSDA for $\text{Ti}_2\text{Mn}_2\text{O}_7$. The upper (lower) panel corresponds to the majority (minority) spin. The negative of density of states has been plotted in the lower panel for clarity. Inset shows minority spin channel density of states for the energy region near Fermi level at ambient and 16.28 GPa. The solid and dashed lines show the contribution from Mn - 3d and Ti-6s+O'-2p states respectively within LSDA.

pressure. Since the underlying mechanism of ferromagnetism is based on the Mn-Ti-O' hybridization, weakening of such hybridization would cause a decrease in T_c as supported by the detail calculation presented above. The change in the hybridization is proportional to the change in the hopping interaction strength, t and inversely to the change in the energy level separation Δ . Application of pressure causes shortening of bondlength, hence one would expect hopping to increase and in turn the hybridization to increase, opposite to what is observed in the calculation. For this we performed the NMTO-downfolding calculation keeping Mn-3d, Ti-6s and O-2p degrees of freedom active and integrating out the rest, including O' degrees of freedom to define a Ti-O' effective level. The real-space representation of that downfolded Hamiltonian in the NMTO-Wannier function basis for $\text{Ti}_2\text{Mn}_2\text{O}_7$ under application of 16.28 GPa pressure shows the Ti-O' effective level to shift down by 0.3 eV compared to that under ambient pressure. This increases the Δ and substantially reduces the Ti-O'-Mn hybridization, substantial enough to compensate the in-

crease in $t_{sd\sigma}$ hopping interaction between Mn- t_{2g} and the effective Tl-s orbital and to produce a net negative contribution to the hybridization. This is an interesting, counter-intuitive situation which can only be unraveled by a detail analysis of the underlying electronic structure as has been done in the present study.

C. Sb-doped $\text{Tl}_2\text{Mn}_2\text{O}_7$

To mimic the doping effect, we have carried out calculations using supercell containing sixteen Mn atoms. Construction of such supercell has been described in section II. Out of these, sixteen Mn atoms, some are substituted by Sb to simulate the effect of doping. There are two doping levels that have been investigated. In one case, one of the Mn atom is substituted by an Sb atom, and in another case, two of the Mn atoms are replaced by two Sb atoms. The former amounts to doping level of $x=0.125$ or 6.25% and the latter amounts to doping of $x=0.25$ or 12.5 %. These are not exactly the doping levels that has been investigated experimentally but close to them (*i.e.* $x = 0.1$ and 0.2 respectively).

Substitution of Mn^{4+} by larger cation Sb^{5+} does not cause any significant changes in the crystal structure, other than the fact that lattice expands slightly keeping the various angles unchanged. The lattice parameters corresponding to doping levels of $x=0.125$ and 0.25 are obtained by interpolation of the experimentally determined lattice constants at various doping as shown in the inset of Fig.1. in ref⁷. The lattice parameters for $x=0.125$ and 0.25 are increased by 0.3% and 0.9% respectively, compared to undoped lattice constant.

To estimate the exchange interaction strengths for $\text{Tl}_2\text{Mn}_{2-x}\text{Sb}_x\text{O}_7$ with $x=0.125$ and 0.25 we have carried out LSDA total energy calculations for various spin arrangements of Mn atoms as explained in section II. The relative LSDA total energies, as given in Table V are mapped on to Eq. (1) in order to extract the J 's. At 6.25

	ΔE (meV)		
	$x=0$	$x=0.125$	$x=0.25$
FM	0	0	0
AFM1	9.55	16.50	23.96
AFM2	13.98	26.07	29.39
AFM3	12.24	23.18	31.53
AFM4	17.59	33.30	35.69
AFM5	18.39	34.39	40.11

TABLE V: Relative LSDA energies per Mn ion in meV in FM and five AFM spin configurations for doped $\text{Tl}_2\text{Mn}_2\text{O}_7$. All energies are converged upto 0.01 meV per Mn ion.

% doping the average coordination numbers change to 5.6, 11.2 and 11.2 respectively. In order to check whether the chosen disordered configuration has any influence on the trend, we have repeated the calculation with two Sb

atoms in the unit cell for two cases. In one case, two Sb atoms were chosen as NN pairs while in the second case they have been chosen as 3NN pairs. The respective coordination numbers at 12.5 % doping are 5.14, 10.28 and 10.86 for 3NN substitution and 5.28, 10.28 and 10.28 for NN substitution. In all the three cases, *i.e.* for $x=0.125$, 0.25 (NN) and 0.25 (3NN), the ground state is found to be FM.

doping	J_1	J_2	J_3	J_0	$D(E_F)$	T_c^{mf}
conc.	(meV)	(meV)	(meV)	(meV)	(States/eV)	(K)
$x=0.0$	-2.52	-0.11	+0.33	-12.48	0.2	181
$x=0.125$	-3.65	-0.12	-0.41	-26.38	1.0	382
$x=0.25(3\text{NN})$	-2.72	-0.57	-0.85	-29.08	1.4	422
$x=0.25(\text{NN})$	-2.74	-0.56	-0.87	-29.30	1.44	423

TABLE VI: Exchange interaction strengths J_1 (NN), J_2 (2NN) and J_3 (3NN) and effective exchange coupling strength J_0 in meV, total density of states at Fermi level, $D(E_F)$ and mean-field Curie Temperature, T_c^{mf} for $\text{Tl}_2\text{Mn}_{2-x}\text{Sb}_x\text{O}_7$, $x=0.0$, 0.125 and 0.25 .

Table VI gives the magnetic exchange interaction strengths for all the three cases and their corresponding T_c 's and density of states at E_F , $D(E_F)$. For comparison, we also quote the numbers corresponding to pure $\text{Tl}_2\text{Mn}_2\text{O}_7$ taken from ref⁹. Pristine $\text{Tl}_2\text{Mn}_2\text{O}_7$ has a very strong NN FM interaction, a weak 2NN FM interaction and a little stronger 3NN AFM interaction. With the introduction of doping, all the interactions became FM and their strengths also increase. On further increase of doping, the 2nd and 3NN FM interactions become stronger with a small decrease in the NN FM interaction. It is worth mentioning here that the results for $x=0.25$ doping with two NN Mn atoms substituted, does not change significantly compared to the result when the two Mn ions substituted were 3NNs, proving that choice of disordered configuration does not alter the general trend. Computation of T_c , using the values of J_1 , J_2 and J_3 , listed in Table I, show rapid increase in T_c on the initial doping which then attains a kind of saturation on further doping, considering upto moderate level of doping. This trend is in good agreement with experimental findings, but the quantitative values differ. This happens primarily because of the clustering effect not included in our calculation. To quote Alonso *et. al.*⁷, “For low doping levels, we cannot disregard some type of magnetic clustering with almost pure $\text{Tl}_2\text{Mn}_2\text{O}_7$ ($T_c = 135\text{K}$) and Sb rich regions”. Such effects are bound to reduce the global T_c measured experimentally. Also lattice relaxation effect could be important. Although experimentally measured crystal structure data shows the same space group symmetry as that of the undoped one with little variation in the internal u parameter, the substitution of Mn ion by a larger cation will probably change the structure locally. Therefore structural relaxations of the doped compounds, which is beyond the scope of our present computational capacity, are needed to resolve the

issue completely.

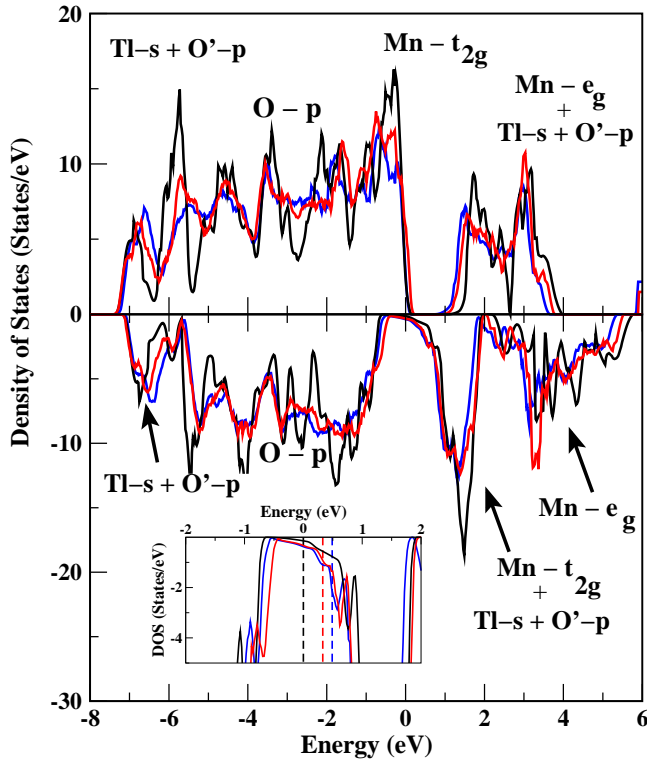


FIG. 7: (color on-line) Spin-decomposed density of states for $x=0.0$ (black), 0.125 (red) and 0.25 (blue) doping in $\text{Tl}_2\text{Mn}_{2-x}\text{Sb}_x\text{O}_7$. Zero of the energy is set at the Fermi level of the undoped $\text{Tl}_2\text{Mn}_2\text{O}_7$ compound. The upper (lower) panel corresponds to the majority (minority) spin. The negative of density of states has been plotted in the lower panel for clarity. Inset shows the density of states in minority spin channel at the same doping levels for the energy region close to Fermi level. The dashed lines in the inset correspond to the respective Fermi levels.

One needs to examine the electronic structure upon doping to understand the microscopic origin of the striking effect described above. In Fig. 7 we show the density of states corresponding to Sb-doped $\text{Tl}_2\text{Mn}_2\text{O}_7$ for doping level of $x=0.125$ and 0.25 . To appreciate the changes in the electronic structure upon doping, we also show the density of states for pure $\text{Tl}_2\text{Mn}_2\text{O}_7$. Comparing the various density of states, we observe slight shrinking of the overall band-width due to the small expansion of the lattice. The t_{2g} - e_g splitting at the Mn site decreases due to expansion of the Mn-O bondlength. Smearing of the DOS, compared to pure case is also observed due to the effect of disordering. The Sb ions in the $5+$ state have completely filled $4d$ shell which are essentially core-like while $5s$ and $5p$ states remain more or less empty with no contribution to the states close to E_F . The most important effect is that of electron doping. Replacement of Mn^{4+} by Sb^{5+} introduces additional electrons in the system which have no other option but to populate the

highly dispersive $\text{Tl-O}'\text{-Mn-}t_{2g}$ hybrid state in the minority spin channel. Because of the highly dispersive nature of this band, the density of state in the minority spin channel close to E_F rises fast after the tail part which then attains a kind of small plateau before attaining highly peaked values corresponding to weakly dispersive Mn t_{2g} dominated states between 1 - 2 eV. This is shown in the inset of Fig.7. With introduction of first Sb atom, the doped extra electrons while populating the dispersive minority spin band increases $D(E_F)$ substantially. Upon increasing the number of Sb atoms from one to two, the Fermi level shifts towards right to accommodate more electrons, but since it has almost crossed the highly dispersive region and falls within the plateau-like structure, $D(E_F)$ does not change significantly. This is evident by quantitative estimates of $D(E_F)$ shown in Table I. In Fig.7, we have shown only the case of $x=0.25$ (NN), but the DOS corresponding to $x=0.25$ (3NN) is not very different and $D(E_F)$ changes only marginally. Following the perturbative treatment in terms of the transfer integral²⁶, t , between the magnetic and nonmagnetic site, the exchange coupling, J , within the proposed kinetic energy driven scheme is given by, $t^4 D(E_F)/\Delta^2$, where Δ is the average energy separation between the magnetic and nonmagnetic level and $D(E_F)$ is the density of states at Fermi level introduced in the above. The real space representation of NMTO-downfolded Hamiltonian keeping Tl-6s, Mn -3d and O-2p states active and downfolding the rest shows that the Tl-Mn hopping integral, t 's and their energy level separation changes only slightly for 0.3% and 0.9% expansion of the lattice upon $x=0.125$ and 0.25 doping. The major changes come from the sharp increase in $D(E_F)$ which explains the enhancement of J 's and T_c 's in turn.

IV. CONCLUSIONS

We presented a detailed study of $\text{Tl}_2\text{Mn}_2\text{O}_7$ under pressure and Sb-doped $\text{Tl}_2\text{Mn}_2\text{O}_7$ using first-principles electronic structure calculations. The analysis of the computed electronic structure shows that the counter-intuitive experimental observation of suppression of ferromagnetic T_c upon application of pressure and its enhancement upon moderate amount of doping by Sb in Mn sublattice is naturally explained in terms of the hybridization induced mechanism proposed earlier⁹. Application of pressure reduces the hybridization between localized Mn t_{2g} level and the delocalized $\text{Tl-O}'$ effective state due to the shifting of the position of the $\text{Tl-O}'$ effective level, which weakens the driving mechanism of ferromagnetism and thereby reduces the strength of exchange coupling and the T_c .

In case of doping, on the other hand, the enhancement of T_c is induced by the charge-carrier doping of the system by Sb. This enhances the value of density of states at the Fermi energy significantly, thereby enhancing the exchange coupling and the T_c . Our conclusions were substantiated by the explicit calculation of the J's and the T_c 's.

In case of $\text{Ti}_2\text{Mn}_2\text{O}_7$ under pressure, we resolved the issue related to the change in Mn-O-Mn angle. We carried out structural relaxation by means of accurate pseudopotential based total energy calculations. Our theoretical results show, as opposed to the claim by Velasco *et al.*¹⁵, the Mn-O-Mn angle decreases in agreement with the original suggestion by Sushko *et al.*⁶. However the

decrease is only marginal and for all practical purposes, it may be assumed to remain same as that of $\text{Ti}_2\text{Mn}_2\text{O}_7$ in ambient condition. This rules out the use of angle variation argument to explain the reduction of T_c .

Acknowledgements

The research was funded by DST project SR/S2/CMP-42/2003. We thank MPG-partnergroupprogram for the collaboration.

-
- * Also at Jawaharlal Nehru Center for Advanced Scientific Research and Center for Condensed Matter Theory, IISc, Bangalore, India.
- ¹ H. Y. Hwang and S. -W. Cheong, *Nature*(London) **389**, 942 (1997)
 - ² Y. Shimakawa, Y. Kubo and T. Manako, *Nature*(London) **379**, 53 (1996).
 - ³ H. Okamura, T. Koretsune, M. Matsunami, S. Kimura, T. Nanba, H. Imai, Y. Shimakawa and Y. Kubo, *Phys. Rev. B* **64** 180409(R) (2001).
 - ⁴ J. Sanchez-Benitz, A. de Andres, C. Prieto, J. Avila, L. Martin-Carron, J. L. Martinez, J. A. Alonso, M. J. Martinez-Lope and M. T. Casais, *Appl. Phys. Lett.* **84** 4209 (2004).
 - ⁵ A. Ramirez and M. A. Subramanian, *Science* **277**, 546 (1997).
 - ⁶ Yu. V. Sushko, Y. Kubo, Y. Shimakawa and T. Manako, *Physica B* **259-261**, 831 (1999).
 - ⁷ J. A. Alonso, M. J. Martínez-Lope, M. T. Casais, P. Velasco, J. L. Martínez, M. T. Fernandez-Díaz and J. M. de Paoli, *Phys. Rev. B* **60**, R15024 (1999).
 - ⁸ O. K. Andersen and T. Saha-Dasgupta, *Phys. Rev. B* **62**, R16219 (2000); O. K. Andersen, T. Saha-Dasgupta and S. Ezhov, *Bull. Mater. Sci* **26**, 19 (2003) and references therein.
 - ⁹ T. Saha-Dasgupta, M. De Raychaudhury and D. D. Sarma, *Phys. Rev. Lett.* **96**, 087205 (2006).
 - ¹⁰ M. D. Núñez-Regueiro and G. Lacroix, *Phys. Rev. B* **63**, 014417 (2000).
 - ¹¹ D. D. Sarma, Priya Mahadevan, T. Saha-Dasgupta, Sugata Ray and Ashwani Kumar, *Phys. Rev. Lett* **85**, 2549 (2000).
 - ¹² D. D. Sarma, *Current Opinion in Solid State & Materials Science* **5**, 261 (2001).
 - ¹³ P. Mahadevan, A. Zunger and D. D. Sarma, *Phys. Rev. Lett.* **93**, 177201 (2004).
 - ¹⁴ Y. Shimakawa, Private Communication, $\angle\text{Mn-O-Mn}$ decreases in the small experimental pressure range.
 - ¹⁵ P. Velasco, J. A. Alonso, V. G. Tissen, W. G. Marshall, M. T. Casais, M. J. Martínez-Lope, A. de Andres, C. Prieto and J. L. Martínez, *Phys. Rev. B* **67**, 104403 (2003).
 - ¹⁶ O. K. Andersen and O. Jepsen, *Phys. Rev. Lett.* **53**, 2571 (1984).
 - ¹⁷ N. M. Rosengaard and B. Johansson, *Phys. Rev. B* **55** 14975 (1997)
 - ¹⁸ X. Wan, M. Kohno and X. Hu, *Phys. Rev. Lett.* **94** 087205 (2005)
 - ¹⁹ M. A. Subramanian, B. H. Toby, A. P. Ramirez, W. J. Marshall, A. W. Sleight and G. H. Kwei, *Science* **273**, 81 (1996).
 - ²⁰ D. Vanderbilt, *Phys. Rev. B* **41**, R7892 (1990).
 - ²¹ G. Kresse and J. Hafner, *Phys. Rev. B* **47**, 558 (1993); G. Kresse and J. Furthmüller, *Comput. Mater. Sci.* **6**, 15 (1996); *ibid* *Phys. Rev. B* **54**, 11169 (1996).
 - ²² P. E. Blöchl, *Phys. Rev. B* **50**, 17953 (1994); G. Kresse and J. Joubert, *Phys. Rev. B* **59**, 1758 (1999).
 - ²³ F. D. Murnaghan, *Proceedings of the National Academy of Science* **30**, 244 (1944).
 - ²⁴ The importance of Ti-O-Mn hybridization has also been indicated earlier by C. I. Ventura and B. Alascio [*Phys. Rev. B* **56**, 14533 (1997)] and by Y. Shimakawa, Y. Kubo, N. Hamada, J. D. Jorgensen, Z. Hu, S. Short, M. Nohara and H. Takagi [*Phys. Rev. B* **59**, 1249 (1999)].
 - ²⁵ M. De Raychaudhury, T. Saha-Dasgupta and D. D. Sarma, unpublished.
 - ²⁶ J. Kanamori and K. Terakura, *J. Phys. Soc. Jpn.* **70**, 1433 (2001).
 - ²⁷ C. J. Fennie and K. M. Rabe, *Phys. Rev. B* **72**, 214123 (2005).